Sub-Surface, Micrometer-Scale Incisions Produced in Rodent Cortex using Tightly-Focused Femtosecond Laser Pulses

John Nguyen,[1] Jillian Ferdman,[1] Mingrui Zhao,[2] David Huland,[1] Shatha Saqqa,[1] Jan Ma,[1] Nozomi Nishimura,[1] Theodore H. Schwartz,[2] and Chris B. Schaffer[1]*

[1]*Department of Biomedical Engineering, Cornell University, Ithaca, New York 14853*
[2]*Department of Neurological Surgery, Weill Cornell Medical College, New York, New York 10065*

Background and Objective: Techniques that allow targeted, micrometer-scale disruption in the depths of biological tissue, without affecting overlying structures or causing significant collateral damage, could potentially lead to new surgical procedures. We describe an optical technique to make sub-surface incisions in *in vivo* rodent brain and characterize the relationship between the cut width and maximum depth of these optical transections as a function of laser energy.

Materials and Methods: To produce cuts, high intensity, femtosecond laser pulses were tightly focused into and translated within the cortex, through a craniotomy, in anesthetized rodents. Imaging of stained brain slices was used to characterize cut width and maximum cutting depth.

Results: Cut width decreased exponentially as a function of depth and increased as the cube root of laser energy, but showed about 50% variation at fixed depth and laser energy. For example, at a laser energy of 13 μJ, cut width decreased from 158 ± 43.1 μm (mean ± standard deviation) to 56 ± 33 μm over depths of approximately 200–800 μm, respectively. Maximal cut depth increased logarithmically with laser energy, with cut depths of up to 1 mm achieved with 13 μJ pulses. We further showcased this technique by selectively cutting sub-surface cortical dendrites in a live, anesthetized transgenic mouse.

Conclusions: Femtosecond laser pulses provide the novel capacity for precise, sub-surface, cellular-scale cuts for surgical applications in optically scattering tissues. Lasers Surg. Med. 43:382–391, 2011. © 2011 Wiley-Liss, Inc.

Key words: photodisruption; laser ablation; animal models; nonlinear optical absorption; nonlinear optics; nonlinear microscopy; two-photon microscopy

INTRODUCTION

Tools that enable the disruption of targeted structures in the bulk of a biological tissue without affecting the overlying structures or causing collateral damage outside the targeted volume could open the door to new surgical procedures. Radio-frequency and ultrasound ablation enable sub-surface incisions, but have a spatial precision of centimeters to millimeters, respectively [1,2]. Mechanical tools, such as scalpels, can achieve higher cutting precision, but incisions must start at a tissue surface. What is lacking is a technique that provides spatial precision comparable to or better than a mechanical scalpel, with the ability to disrupt sub-surface structures and preserve the overlying tissue.

Nonlinear optical absorption can enable fine-scale, sub-surface disruption in biological tissue. In most biological samples, linear absorption of near-infrared light is weak, so this light can penetrate deeply into the tissue. Focusing femtosecond-duration pulses of near-infared light at high numerical aperture into the bulk of the tissue produces high intensities that can drive nonlinear absorption of the laser energy in the focal volume. Multiphoton and tunneling ionization produce initial ionized electrons which then linearly absorb laser energy and impact ionize other electrons, a process called avalanche ionization [3]. When using lower energy pulses from high-repetition rate laser sources in the MHz range, tissue damage from this nonlinear absorption is likely dominated by cumulative photochemical damage [4] and heat accumulation [5]. In contrast, when using higher energy pulses from lower repetition rate laser sources of around 1 kHz, damage is largely driven by vaporization of tissue components in the focal volume and subsequent mechanical effects such as cavitation [4,6]. In this regime, sufficient ionization occurs to cause optical breakdown and plasma formation, vaporizing material in the focal volume. The subsequent expansion of the vaporized material leads to the formation of a cavitation bubble and the launch of a propagating pressure wave [4,7]. The maximal expansion of this cavitation bubble determines the volume of tissue that is disrupted. In both of these regimes, because nonlinear absorption of the laser energy is localized within the

*Corresponding to: Chris B. Schaffer, Department of Biomedical Engineering, Cornell University, Ithaca, NY 14853.
E-mail: cs385@cornell.edu
Accepted 13 February 2011
Published online 15 June 2011 in Wiley Online Library (wileyonlinelibrary.com).
DOI 10.1002/lsm.21054

focal volume, tissue disruption can be confined to micrometer-sized volumes, while leaving the surrounding tissue intact.

Several studies have used femtosecond laser ablation to disrupt biological structures in a variety of *in vitro* preparations and *in vivo* animal experiments, as well as in humans. Single chromosomes in human cells have been dissected, providing a technique for noninvasive gene inactivation [8] and single cell and sub-cellular disruptions permitted studies that elucidated the functional neural architecture [9] and mechanisms of neural regeneration [10] in *C. elegans*. Ablation of single cells in drosophila embryos was used to study the role of mechanical forces in development [11], while targeting of sub-cellular structures, such as cytoskeletal filaments, in live cells provided insight into the regulation of mechanical stiffness [12,13]. Additionally, femtosecond laser pulses have been used to selectively perforate cellular membranes for DNA transfection [14,15]. Femtosecond lasers are now also routinely used to produce sub-surface cuts in cornea as a means to produce the "flap" necessary for laser-assisted in situ keratomileusis for vision correction surgery [16]. In all these examples, the samples are almost completely transparent and have little to no optical scattering, making the delivery of focused femtosecond pulses to sub-surface regions relatively straightforward. As long as there is not strong linear absorption of the light, however, this approach to producing sub-surface disruption should also be feasible in scattering tissues. Scattered light cannot contribute to nonlinear absorption and has minimal effects on the tissue, so the laser energy incident on the sample can be increased to compensate for scattering losses and deliver the necessary energy to the focus to cause optical breakdown in the depth of the tissue. For example, previous work has shown that it is possible to produce sub-surface ablation in keratinized corneal and scleral tissue, where the tissue is optically scattering [17]. Additionally, rodent models of small stroke have been developed using femtosecond laser ablation to trigger clotting in individually targeted, cortical blood vessels that are located several hundred micrometers in the depth of scattering brain tissue [18]. In other work, individual dendrites were cut from pyramidal neurons in live mouse brain, illustrating the precision possible with femtosecond laser ablation, even in scattering tissue [19].

Here, we used tightly-focused femtosecond pulses as a light scalpel to make sub-surface incisions in *in vivo* rodent brain, a scattering biological tissue. We demonstrated our ability to produce sub-surface cuts by ablating the cortex in the rostral-caudal direction. We then produced vertical cuts to determine cut width and maximum achievable ablation depth as a function of laser energy. We used these results to construct a phenomenological model that predicts the laser energy that should be chosen to achieve a given cut size at a given cortical depth. Overall, we describe a technique that allows ablation of biological structures that lie below the surface of a scattering tissue with cell-level precision.

METHODS

Animal Preparation

Data was acquired from seven male Sprague-Dawley rats (275–350 g). Two rats were used to produce sub-surface, horizontal ablations at constant depths with fixed laser energy (Fig. 2). The remaining rats were used to study depth-dependent cut width and maximum ablation depth as a function of laser energy (Figs. 3 and 4). Briefly, animals were anesthetized by interperitoneal injection of urethane (150 mg/100 g rat). Animals were further supplemented with subcutaneous injections of 5% (wt/vol) glucose in phosphate buffered saline (PBS) every hour (0.5 ml per 100 g rat). Body temperature was maintained at 37°C with a rectal thermometer and heating blanket (50-7053; Harvard Apparatus). Heart rate and arterial blood oxygen saturation were continuously monitored using a pulse oxymeter (MouseOx; Starr Life Sciences Corp.). A 3 × 4 mm craniotomy was prepared over the parietal cortex and the dura was removed. The craniotomy was filled with 1.5% (wt/vol) low-melting temperature agarose (A9793; Sigma) in artificial cerebral spinal fluid and sealed with a glass coverslip (50201; World Precision Instruments) that was fixed to the skull using cyanoacrylate glue and dental cement (Lang Dental Mfg Co. & Co-Oral-Ite Dental Mfg Co.). To fluorescently label the blood plasma, a 0.4 ml bolus of 5% (wt/vol) 2 MDa fluorescein-conjugated dextran (FD2000S; Sigma) in PBS was intravenously injected into the tail vein. All animal procedures were reviewed and approved by the

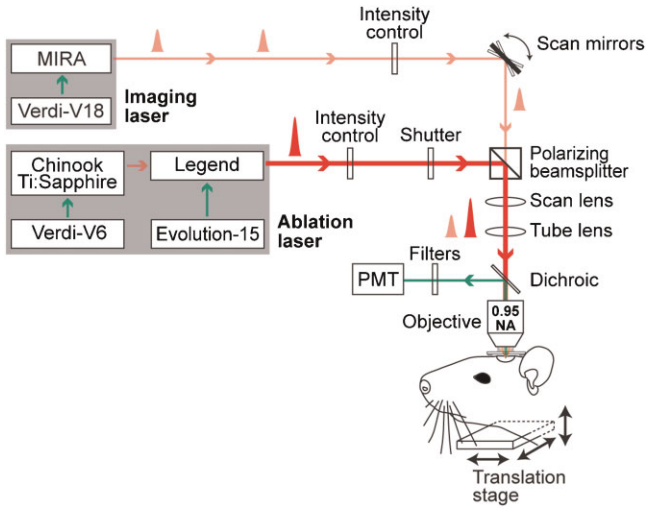

Fig. 1. Optical setup for *in vivo* imaging and ablation. Following the craniotomy, the animal was placed on a translational stage that allowed for navigation of the cranial window. Two-photon images were obtained by raster scanning the window with a high-repetition rate, femtosecond pulse train and collecting the two-photon excited fluorescence with a photomultiplier tube (PMT). Femtosecond laser pulses from a regenerative amplifier used for ablation were combined with the imaging beam using a polarizing beamsplitter to allow for simultaneous imaging and ablation.

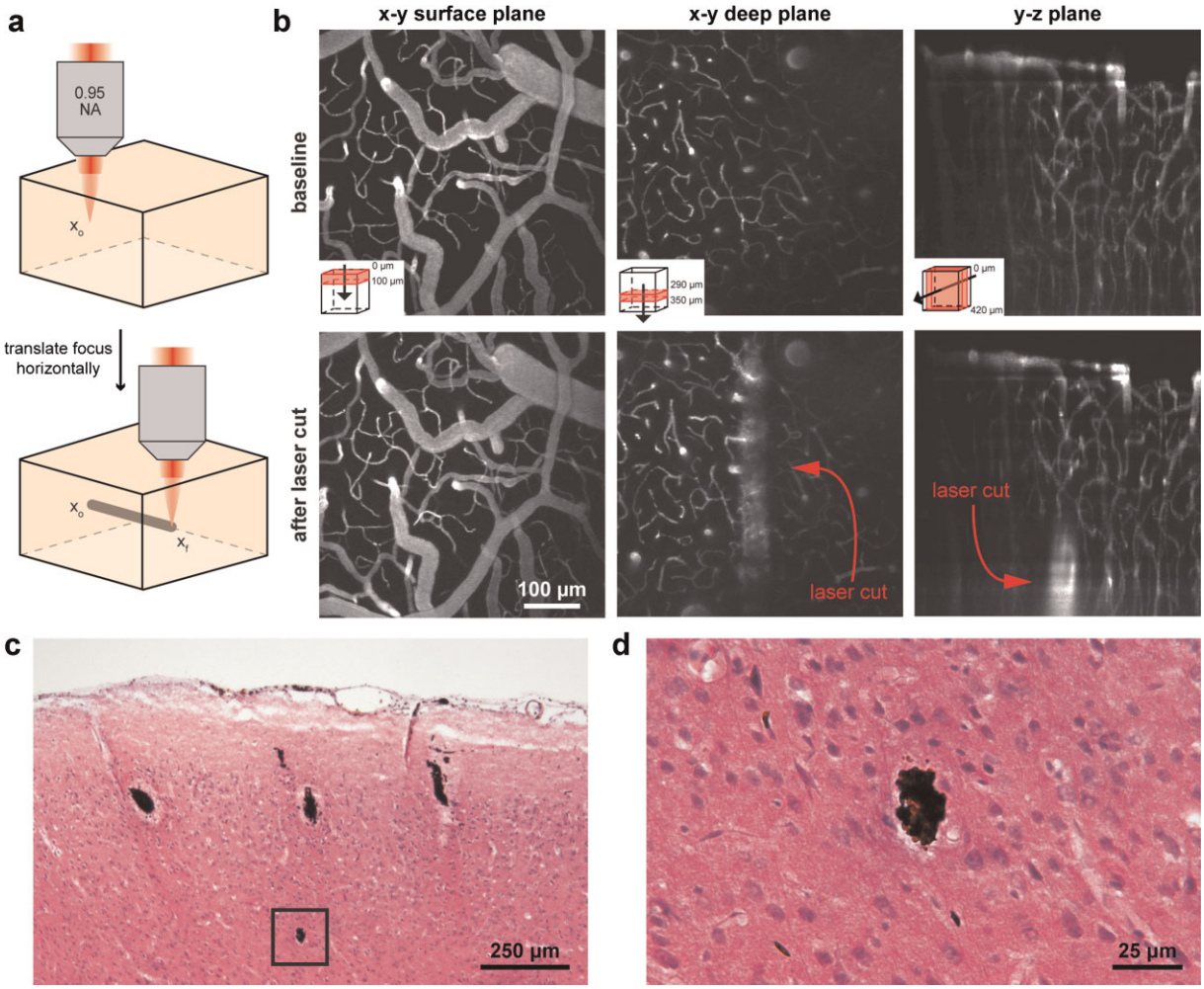

Fig. 2. Sub-surface cuts in rat cortex *in vivo* and in H&E and DAB stained brain slices. (**a**) Subsurface cuts were produced by tightly focusing high-energy, femtosecond laser pulses into the cortex of a live, anesthetized rat, through a craniotomy and translating the rat in the horizontal direction at a constant depth. (**b**) Average projections of two-photon image stacks of fluorescently labeled cortical vasculature at baseline (top) and after laser cut (bottom). Corner schematics indicate direction and volume of projections. The cut was produced with 4.5 μJ laser pulse energy, focused to a depth of approximately 350 μm. Centered around the cut is an approximately 75 μm band of labeled blood plasma from capillaries ruptured during the cutting (middle, bottom). The post-cut images were acquired approximately five minutes after the cut was produced. (**c**) H&E and DAB (for red blood cells) stained 20 μm thick coronal brain slice with sub-surface ablations. Three cuts, produced approximately 300 μm below the surface of the brain with 0.5 μJ laser energy, serve as markers to identify a single cut made at approximately 700 μm below the brain surface with 3 μJ laser energy. (**d**) Higher magnification view of the deeper cut from panel (c) (boxed).

Institutional Animal Care and Use Committee at Cornell University.

Two-Photon Excited Fluorescence Microscopy

Images were obtained with a custom two-photon laser-scanning microscope that was designed to include an amplified laser beam to produce sub-surface ablations (Fig. 1). Low-energy, 800 nm wavelength, 76 MHz femtosecond laser pulse train generated from a commercial Ti:Sapphire laser (Mira-HP; Coherent), pumped by a continuous wave laser (Verdi-V18; Coherent Inc.), was used for two-photon excited fluorescence (2PEF) microscopy. A 0.28 numerical aperture (NA), 4× air objective (Olympus) was used to obtain a map of the surface vasculature across the entire craniotomy (Fig. 3b). A 0.95 NA, 20× water immersion objective (Olympus) was used for high resolution imaging (Fig. 2b and Fig. 5) and producing sub-surface cuts.

Femtosecond Laser Sub-Surface Ablation

For sub-surface ablation, we used high-energy, 800 nm wavelength, 1 kHz repetition rate train of 50 femtoseconds

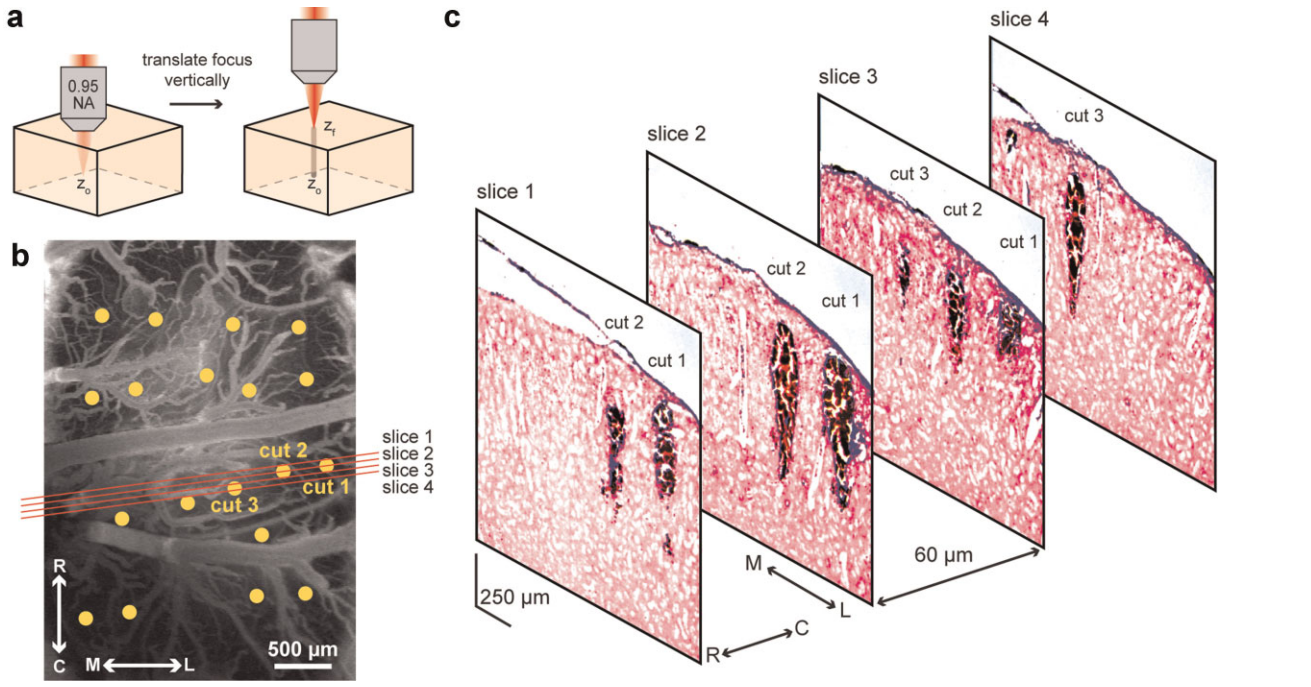

Fig. 3. Vertical cuts are identified in serial brain slices stained with H&E and DAB. (**a**) Schematic of vertical sub-surface ablation. High intensity, femtosecond laser pulses were tightly focused into the brain through a craniotomy, and cuts were made by vertically translating the animal, starting deep within the cortex. (**b**) *In vivo* two-photon image of fluorescently labeled surface vasculature. Yellow dots represent locations where sub-surface cuts were produced. Red lines correspond to histological brain slices in (**c**). The brain was sliced at a tilt due to the angled mounting of the brain on the cryostat. R: rostral, C: caudal, M: medial, L: lateral. (**c**) Serial images of every fourth 20 μm thick brain slice stained with H&E and DAB. Cuts labeled one, two, and three correspond to labeled cut locations in (**b**). Slices one through three reveal the beginning, middle, and end cross-section views of the damage caused by cuts one and two. Slice three shows a beginning cross-section view of cut three, with a middle cross-section view in slice four.

pulses produced by a commercial regenerative amplifier (Legend 1k USP; Coherent) pumped by a Q-switched laser (Evolution 15; Coherent) and seeded by a Ti:Sapphire oscillator (Chinhook Ti:Sapphire laser; Kapteyn-Murnane Laboratories Inc., pumped by Verdi-V6; Coherent Inc.). To produce sub-surface ablation, the amplified pulse train was combined with the imaging laser through the use of a polarizing beamsplitter and was tightly focused into the cortex with a 0.95 NA objective. This allowed for simultaneous, real-time imaging and ablation (Fig. 1). To make cuts, the animal was translated at 50 μm/second either horizontally or vertically relative to the cortex surface, depending on the study, while continuously irradiating with the 1 kHz pulse train. At this translation speed, approximately 20 pulses are deposited in each volume along the cut. For horizontal cuts, translation occurred at constant depth (Fig. 2a). For vertical cuts (Fig. 3a), laser light was focused more than 1 mm into the cortex, and the animal was vertically translated until the focus neared the surface of the brain. For vertical cuts, about 15–20 cuts were placed in each animal in an irregular grid that avoided large blood vessels using laser energies of 0.3, 5, and 13 μJ (Fig. 3b). At the two higher energies, irradiation was halted about 200 μm below the brain surface to prevent rupturing of large surface vessels.

Post-Mortem Histology

At the conclusion of each experiment, animals were euthanized and were perfused with 100 ml PBS followed by 100 ml 4% (wt/vol) paraformaldehyde in PBS. Brains were extracted and post-fixed in 4% paraformaldehyde for at least 24 hours. Brains were then cryoprotected using 25% (wt/vol) sucrose in PBS followed by 50% sucrose in PBS [20]. Prior to cryosectioning, fiducial marks were placed at the edges of the cranial window to help map and locate cuts. The brain was then embedded in a cryomold with Optimal Cutting Temperature Compound (O.C.T. Compound, Tissue-Tek), frozen in dry ice, and cut into 20-μm thick coronal sections on a cryostat (HM 505 E, Microm). Slices were stained with 3,3′-diaminobenzidine (DAB) to detect red blood cells as well as hematoxylin and eosin (H&E) to view tissue structure.

Vertical Cut Measurement and Data Analysis

Slides were imaged and examined using an upright microscope (BX41 with DP70 camera; Olympus). Coronal

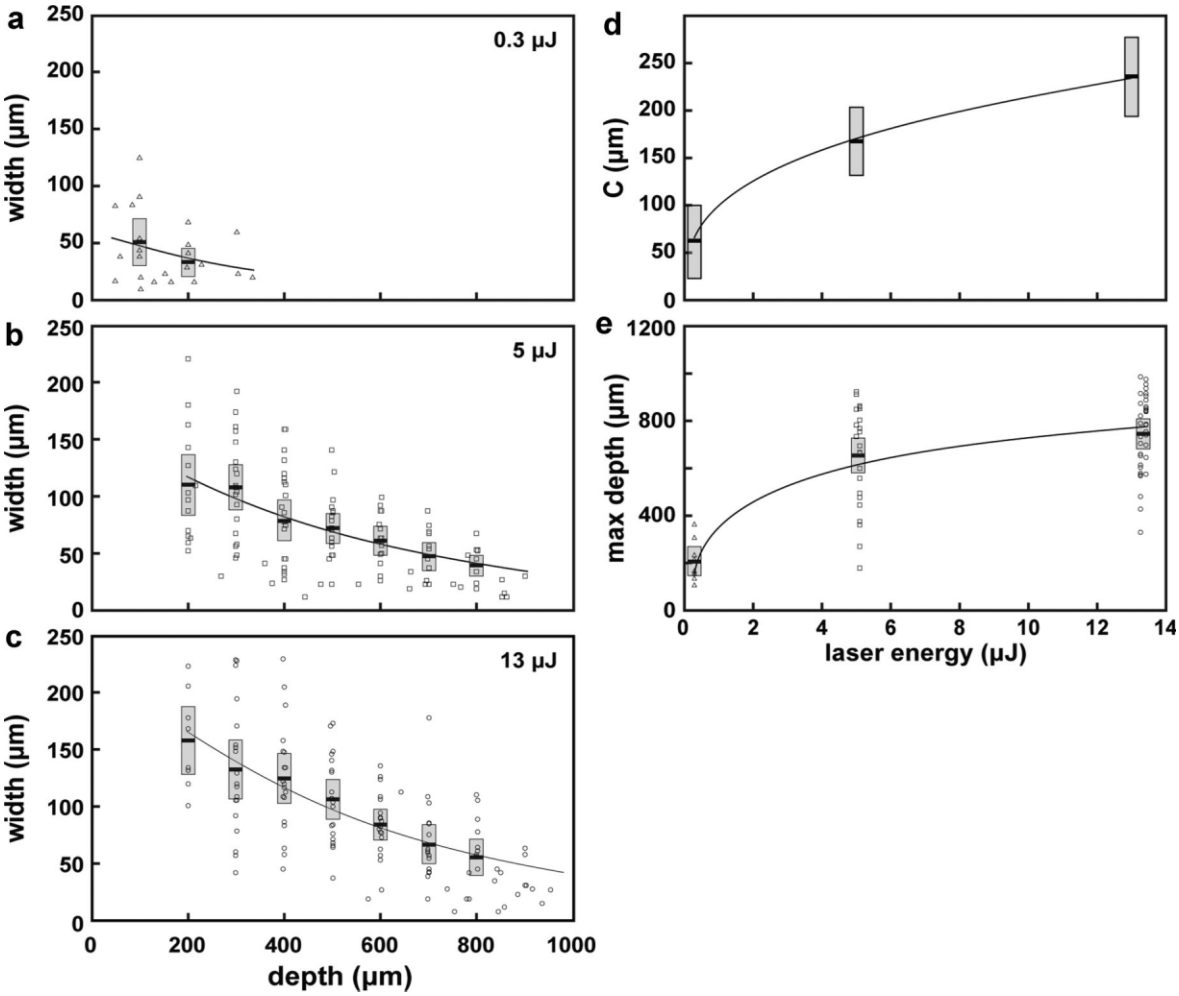

Fig. 4. Dependence of cut width on depth in cortex and laser energy, and dependence of maximum ablation depth on laser energy. Cut width decreases exponentially with depth beneath the cortical surface at laser energies of (**a**) 0.3, (**b**) 5 and (**c**) 13 μJ, with fits to Equation (1) (68 cuts across 5 rats). (**d**) The prefactor in the exponential fits is proportional to cube root of the laser energy (Eq. (2)). (**e**) Maximum cut depth increases logarithmically with laser energy (Eq. (3)). Within all plots, gray boxes represent 95% confidence intervals about the mean, indicated by the horizontal black line. Black trend lines are respective fits for each data set.

sections gave cross-sectional views of cone-shaped, red blood cell-filled cuts. The fiduciary marks and the *in vivo* two photon images were used as guides to help identify specific laser cuts observed in serial brain slices (Fig. 3b and c). For each tissue section that contained a specific cut the width was measured as a function of depth, and this was repeated for every cut. At each depth beneath the cortical surface, the largest width for each specific cut found across all sections that included that cut was used for data analysis. This ensured that the width of the cut was measured at the widest point at each depth. At higher laser energies, cut widths were measured in 100 μm depth increments. Additionally, the maximum cut depth was recorded for each cut. Cut width as a function of depth for each laser energy and the maximum cut depth as a function of laser energy were fitted to quantify trends. For statistical analysis, means were calculated for each binned group as well a 95% confidence interval (CI) about the mean.

Dissection of Neuronal Dendrites in a Transgenic Mouse

We used a 31 g, male, transgenic mouse that expressed yellow fluorescent protein (YFP) in a subset of pyramidal neurons (C57B/6-thy1-YFPH, Jackson Labs) [21] to evaluate structural changes following transections of neural processes using femtosecond laser ablation. The dendritic projections of excitatory pyramidal neurons are imaged in the supragranular layers of the cortex in this mouse line (Fig. 5a). Surgical methods were similar to those described above, with slight modifications. The mouse was anesthetized with 5% inhaled isofluorane, and

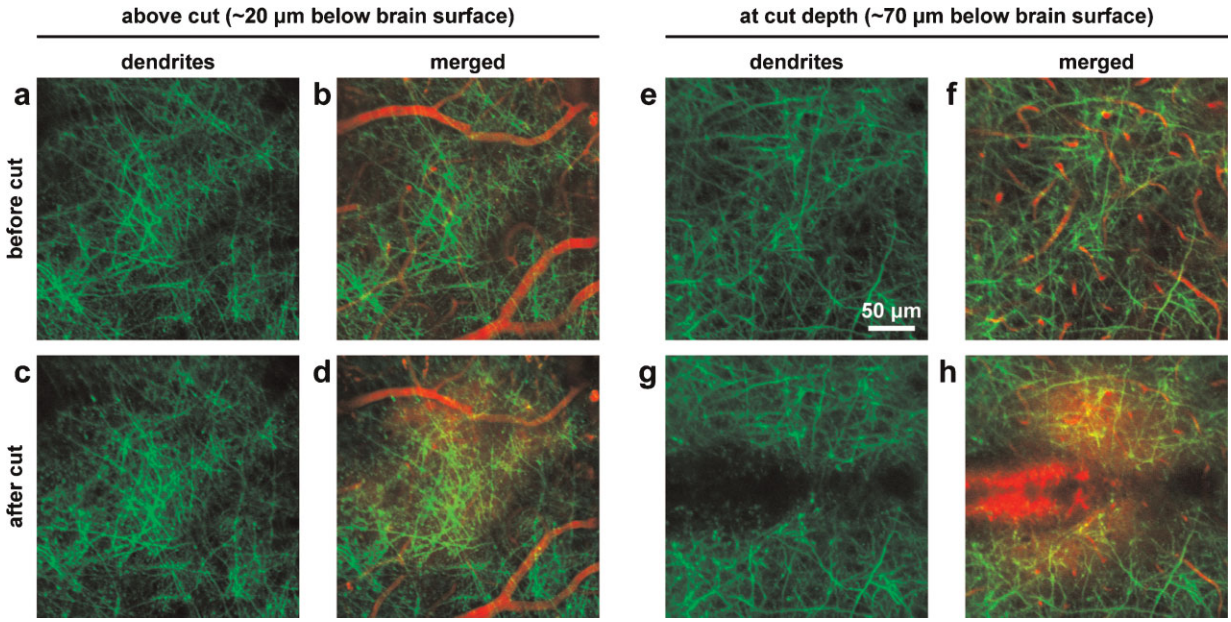

Fig. 5. Femtosecond laser ablation enables sub-surface dissection of neuronal dendrites in a live, anesthetized mouse. Images were obtained from a transgenic mouse that expressed YFP in pyramidal neurons and their dendritic arbors (green). A retro-orbital injection of Texas red-dextran was used to fluorescently label the vasculature (red). Baseline images of dendrites (**a** and **e**) and merged images of both dendrites and capillaries (**b** and **f**) located 20 μm below the brain surface (**a** and **b**) and at the cutting depth of 70 μm (**e** and **f**). A cut was produced with incident laser energy of approximately 0.2 μJ that was translated through the cortex at 50 μm/s. Dendrites and blood vessels above the cut (**c** and **d**) remained unaffected while dendrites were cut and blood vessels were ruptured at the cutting depth (**g** and **h**). Post-cut images were acquired approximately five minutes after the cut was produced.

maintained at approximately 1.25%. We performed a bilateral craniotomy that was sealed with a glass coverslip, leaving the dura intact. To visualize the vasculature, we performed a retro-orbital injection of ~0.4 ml of 2.5% (wt/vol) Texas Red-conjugated dextran (D-1830; Invitrogen) in saline. A 1 mm long medial-lateral cut was produced at a depth of 70 μm with an incident laser energy of ~0.2 μJ in parietal cortex (Fig. 5).

RESULTS

We demonstrated the use of femtosecond laser ablation to produce sub-surface cuts in the cortex of live, anesthetized rodents. 2PEF microscopy was used to monitor cutting in real-time *in vivo*. The cuts were quantified through histological analyses of brain slices. Cut width and maximum achievable ablation depth were measured as a function of laser energy.

Sub-Surface Ablation in Rat Cortex

Two-photon imaging was used to image before, during, and after a sub-surface femtosecond laser cut was produced in the rostral-caudal direction through the cortex of an anesthetized rat with a craniotomy (Fig. 2a). Projections of 2PEF image stacks showed that the surface vasculature (labeled with intravenously injected fluorescein-dextran) was maintained after a horizontal laser cut (Fig. 2b, left). The cut was apparent as a ~75 μm wide fluorescent band in the depth of the tissue, not seen in the baseline image (Fig. 2b, middle). This band was due to fluorescently labeled blood plasma that leaked from the transiently ruptured capillaries that were located along the path of the sub-surface cut. A y–z projection of the vasculature showed that the cut was confined to a volume below the surface of the brain, with the tissue above still intact (Fig. 2b, right).

Histological studies confirmed our ability to produce sub-surface cuts with micrometer precision in the rat cortex. Red blood cells (stained by DAB) were evident in the tissue, confirming that there was some bleeding into the laser cut (Fig. 2c). The width of cuts depended on the laser energy and depth below the cortical surface. In the example of Fig. 2c, three cuts were made with a laser energy of 0.5 μJ near the brain surface that served as guides to help identify a deeper, smaller cortical cut generated with an energy of 3 μJ. Although the laser energy used for the deeper cut was higher compared to the energy used for the shallower cuts, the cut size was smaller due to exponential decay of laser energy as light was focused deeper into the optically scattering brain tissue. A higher magnification view of the 700 μm deep cut showed a 25 μm cut size and an accumulation of red blood cells in the ablated area (Fig. 2d). Because the capillary density is high in the cortex, we found that laser cuts always ruptured enough capillaries to fill the cylinder-

shaped ablated volume with red blood cells. Hematoxylin and eosin staining was used to inspect the surrounding tissue, which appeared intact with very little to no cellular pathology outside the deeper laser cut (Fig. 2d). The larger, shallower cuts showed some hematoxylin destaining in a band around the cut, suggesting cells around the cut volume were damaged when a laser energy that was high for the depth beneath the surface was used.

Depth Dependence of Cut Size and Maximum Achievable Cutting Depth

To determine dependence of the cut width on cortical depth and laser energy as well as the dependence of the maximum ablation depth on laser energy, we produced vertical cuts using different laser energies and analyzed the size of the cuts as a function of depth with histology (Fig. 3a). The location of individual cuts were noted on 2PEF images of the surface vasculature (Fig. 3b) and were mapped to the damage tracts observed in H&E and DAB stained coronal histological sections (Fig. 3c).

We found that for fixed laser energy, the cut width increased as the laser focus was vertically translated from deeper to shallower in the cortex (Fig. 4a–c). For each cut, the width was measured as a function of depth, with the cut width taken to be the maximum width across all serial slices containing a given cut at a particular depth. We found that for all energies, cut widths decreased exponentially with increasing depths. For example, at laser energy of 13 μJ, widths decreased from 158 ± 43.1 μm (mean ± standard deviation) to 56 ± 33 μm for depths of 200–800 μm, respectively. Averaging across all cuts, we found about 50% variation in cut width at a fixed depth and laser energy. Because the maximal extent of the tissue disruption should depend on the maximal size the laser-produced cavitation bubble reaches, the volume of the tissue disrupted should scale approximately linearly with the laser energy deposited into the focal region by nonlinear absorption [4]. For pulse energies above the breakdown threshold, the fraction of the pulse energy that is deposited by nonlinear absorption increases slowly with pulse energy [3]. Thus the width of the laser cut should scale as the cube root of the laser energy that reaches the focus unscattered, which is an exponential function of depth beneath the cortical surface. We thus fit the measured cut width, w, as a function of depth, d, for multiple cuts at each laser energy to

$$w = C \exp\left(\frac{-d}{3l_s}\right) \tag{1}$$

where C is a pre-factor that depends on hydrostatic and vapor pressures and on laser energy, as described by Vogel *et al*. [22] (Fig. 4a–c). The scattering length, l_s, in brain for 800 nm light was taken to be 175 μm [23]. These exponential fits generated pre-factor values of approximately 61, 167, and 235 μm for laser energies 0.3, 5.0, and 13.0 μJ, respectively (Fig. 4d). The pre-factors scaled as the cube root of laser energy, consist with the idea that a roughly constant fraction of the laser pulse energy is deposited into the sample by nonlinear absorption over this range of laser energy. We find that

$$C = 99\,\mu\mathrm{m}/\mu\mathrm{J}^{1/3}\,E^{1/3} \tag{2}$$

where E is the incident laser energy (Fig. 4d). Equations (1) and (2) provide a quantitative formula to predict cut width as a function of laser energy and depth within cortex.

The maximum depth where laser damage was observed was characterized for each cut (Fig. 4e). Ablation will occur as long as the laser energy exceeds the threshold energy for optical breakdown in brain, E_{th}, so the maximum achievable ablation depth, d_{max}, increases logarithmically with laser energy as

$$d_{max} = l_s \ln\left(\frac{E}{E_{th}}\right) \tag{3}$$

Fitting to our experimental data gave a threshold energy of approximately 130 nJ, which corresponds to a fluence of 90 J/cm^2, assuming diffraction-limited focusing (Fig. 4e). This likely significantly overestimates the threshold fluence, as the focusing was unlikely to be diffraction limited deep inside the heterogeneous, scattering brain tissue.

Femtosecond Laser Cutting of Neuronal Dendrites

We produced sub-surface horizontal cuts in the brain of a live, anesthetized mouse that expressed YFP in a subset of pyramidal neurons and imaged the effect on cortical dendrites using 2PEF microscopy. The cuts were placed approximately 70 μm beneath the brain surface and transected the dendritic projections of the pyramidal cells (Fig. 5). Dendrites and blood vessels above the targeted depth were unaffected (Fig. 5a–d), while cut dendrites and bleeding from ruptured capillaries was observed in the plane of the cut (Fig. 5e–h). Although the dendrites and vessels above the cut are intact, leaked plasma caused by the shallow cut was observed (Fig. 5d). Dendrites immediately outside the ablated volume did not show signs of degeneration or blebbing characteristic of acute cellular injury (Fig. 5g).

DISCUSSION

We demonstrated the ability to produce localized, micrometer-scale, sub-surface cuts in rodent cortex using high-energy, tightly-focused, femtosecond laser pulses (Figs. 2 and 5). We measured the cut width as a function of depth in the tissue and the incident laser energy as well as the maximum achievable cutting depth as a function of energy (Fig. 3). We showed that the cut width decreases exponentially with depth and increases as the cube root of the laser energy, while the maximum achievable cut depth increases logarithmically with laser energy (Fig. 4). Overall, our results establish the capability of femtosecond laser ablation to produce disruption beneath the surface of optically scattering tissue. In addition our work

provides a phenomenological guide to what laser energy should be chosen to produce a cut of specified width at a particular cortical depth (Eqs. (1) and (2)), and what ablation depths can be achieved (Eq. (3)).

The width of the laser cuts varied by about 50% at fixed laser energy and depth (Fig. 4a–c). Such variations were likely due to heterogeneity in the vasculature on the surface of the cortex through which the laser beam passed. For example, a large vessel that partially obscures the path of the focused laser beam will attenuate some of the laser energy, due to light absorption and strong scattering by red blood cells [24]. This will reduce the amount of light that reaches the focus, thereby decreasing the size of the cut that is produced.

The maximal achievable ablation depth is ultimately limited by optical scattering. Linear absorption of the laser light could also play a role, but the only significant chromophore in the brain for 800 nm light is the hemoglobin in the red blood cells. The vasculature occupies about 6% of the cortical volume [25], yielding an absorption length of approximately 8 cm, assuming uniformly distributed blood vessels, filled with 2 mM hemoglobin, in tissue with the absorption of water [26,27]. This absorption length is significantly longer than the 175 μm scattering length, so the effects of linear absorption can effectively be ignored, except for the locally strong absorption (and scattering) from large surface blood vessels that was noted above as a potential source of cut heterogeneity.

As the focus penetrates deeper into the tissue the laser power must be increased exponentially to compensate for the scattering loss and maintain enough intensity at the focus to cause optical breakdown. On the other hand, the increase in intensity at depth compared to the surface due to focusing is only a power law with focusing depth. Thus, in order to maintain the same intensity at the laser focus with increasing depth, there is an increase in the intensity at the surface. Eventually, a depth is reached where the intensity at the focus is less than the intensity at the surface of the tissue. At this point, nonlinear absorption will occur at the surface rather than at the focus, prohibiting ablation in the depth. To ensure that ablation is occurring at the focus, the probability of nonlinear absorption at the focus, P_{focus}, must be greater than the probability of absorption at the surface, P_{surface}, giving the condition

$$\frac{P_{\text{focus}}}{P_{\text{surface}}} = \left(\frac{I_{\text{focus}}^N V_{\text{focus}}}{I_{\text{surface}}^N V_{\text{surface}}}\right) \geq 1 \tag{4}$$

where I is the laser intensity, V is the volume, and N is the number of photons which must be simultaneously absorbed to ionize an electron. We approximate the focal volume as a cylinder with diffraction-limited dimensions. Following the analysis of Theer *et al*., we take the volume for nonlinear absorption at the surface to be a product of the beam cross-section at the surface ($A_{\text{surface}} = \pi z^2(\text{NA})^2/n^2$) and the scattering length, as the probability of out-of-focus nonlinear absorption will drop dramatically with increasing depth below the surface due to light scattering [28]. This yields

$$\frac{P_{\text{focus}}}{P_{\text{surface}}} = \left(\frac{2\text{NA}^2 z}{n^2\lambda}\right)^{2N-2} \left(\frac{2\pi n^2\lambda}{\text{NA}^2 l_s}\right) e^{\frac{-Nz}{l_s}} \tag{5}$$

where NA is the numerical aperture of the objective lens, z is the depth of the laser focus beneath the cortical surface, and λ is the wavelength of the light. Breakdown thresholds of biological specimens have been shown to be similar to water [29]. Therefore, we assume that for optical breakdown to occur, the nonlinear absorption of photons must overcome the 6.5 eV bandgap of water. At 800 nm, with a photon energy of 1.56 eV, at least $N = 5$ photons must be simultaneously absorbed in order to overcome the energy bandgap. We assume that these initial seed electrons, generated by multiphoton absorption, can then facilitate avalanche ionization that leads to optical breakdown and damage [4]. In our case, we use an objective lens with an NA of 0.95, an index of refraction of 1.33, an 800 nm wavelength, and a scattering length of 175 μm, which gives a maximum ablation depth of 2.1 mm. In our experimental work, we achieved a maximum ablation depth of about 1 mm beneath the cortical surface using 13 μJ laser pulse energy (Fig. 4e), and thus did not reach this fundamental limit, but were rather limited by the maximum laser energy we used (and the 2 mm working distance of the objective). We did not observe ablation at the sample surface even with the highest energy, supporting the idea that deeper ablation could be achieved with higher laser energy. Using longer laser wavelengths could likely extend the maximum ablation depth even further. At 1300 nm wavelength, the scattering length is longer by about a factor of two in brain [30], but water absorption has not yet become significant. Using this wavelength would increase the maximum achievable ablation depth predicted by Equations (4) and (5) to 4.8 mm, assuming $N = 7$. This analysis neglects the role of tunneling ionization in producing the initial electrons that seed avalanche ionization and treats the initial electron generation as a pure multiphoton absorption process [3]. For the high-order multiphoton ionization considered here, this assumption likely underestimates the nonlinear ionization rate and, therefore, somewhat overestimates the maximal possible ablation depth.

In the sub-surface incisions we produced, capillaries were ruptured, pushing red blood cells and plasma into the brain tissue (Figs. 2 and 5). This bleeding could trigger inflammatory responses and previous work has suggested that blood products can be epileptogenic [31]. The rupturing of capillaries could be avoided by turning off the cutting laser with a mechanical shutter when the laser focus reaches a vessel. This could be achieved, for example, by detecting 2PEF of intravenously injected fluorescein-dextran generated by a lower intensity femtosecond laser focused just ahead of the cutting laser.

With the ability to produce minimal collateral damage, femtosecond laser ablation is an ideal tool for fine-scale

surgery. In addition to sub-surface tissue disruption in non-scattering tissue for ophthalmic surgery [16], femtosecond ablation has also been investigated for surface ablation of tissues, such as teeth and ear [32], showcasing its potential in the clinical setting. We have demonstrated the ability to cut sub-surface, cortical dendrites in optically-scattering brain tissue in live, anesthetized rodents (Fig. 5). This capability may open the door for the use of femtosecond laser ablation in the neurosurgical field. One exciting opportunity is in the treatment of focal cortical epilepsy, where this sub-surface laser ablation technique provides a potential path to stop seizures from starting or spreading without damaging the brain's ability to process information. Because seizures spread horizontally through the brain, while much of normal information processing is associated with vertical connections in the brain, making cuts that encircle regions of the brain where seizures start could prevent the seizure from reaching other parts of the brain while minimally affecting the connections more responsible for normal function. Indeed, a mechanically-based implementation of this surgical therapy, called multiple subpial transactions, has been used to treat human epilepsy. In this method, a small hook wire is used to produce full cortical thickness cuts with 5 mm spacing within the epileptic focus [33]. The technique is crude and results have been mixed, in large part due to extensive collateral damage [34,35]. Multiple small optical transactions could be more effective. In addition to blocking propagation of seizures, isolating microcolumns of epileptic cortex could prevent the coalescence of microseizures into a symptomatic seizure, again with minimal damage to vertical cortical connections [36]. Because this optical ablation technique provides extremely high cutting precision, collateral effects on surrounding tissue would be minimal, resulting in a better preservation of normal function and leading to improved patient outcomes as compared to current surgical approaches for epilepsy treatment.

Overall, our work utilizes nonlinear optical techniques to produce micrometer-scale incisions in the cortex of live, anesthetized rodents. While laser-based therapies in the neurosurgical field have been attempted for decades [37], the precision and sub-surface targeting achieved here were not possible with previous approaches. Additionally, our nonlinear techniques produce significantly less collateral damage than previous techniques that relied on linear absorption. We recognize that not all neurosurgical procedures will require such fine-scale tissue disruption, but for surgical procedures that do require such high precision and sub-surface targeting, femtosecond laser ablation provides an attractive approach.

ACKNOWLEDGMENTS

We thank Prof. Rafael Yuste for early inspiration on the use of this sub-surface cutting tool in brain surgery. This work was funded by grants from the American Society for Laser Medicine and Surgery (C.B.S. and T.H.S.) and the Davis Foundation (C.B.S. and T.H.S.) as well as an NSF GK-12 fellowship (J.N.). Finally, we thank Coherent Inc. for the loan of laser equipment.

REFERENCES

1. Anzai Y, Lufkin R, DeSalles A, Hamilton DR, Farahani K, Black KL. Preliminary experience with MR-guided thermal ablation of brain tumors. Am J Neuroradiol 1995;16(1): 39–48.
2. Kennedy JE. High-intensity focused ultrasound in the treatment of solid tumours. Nat Rev Cancer 2005;5(4):321–327.
3. Schaffer CB, Brodeur A, Mazur E. Laser-induced breakdown and damage in bulk transparent materials induced by tightly focused femtosecond laser pulses. Meas Sci Technol 2001;12(11):1784–1794.
4. Vogel A, Noack J, Huttman G, Paltauf G. Mechanisms of femtosecond laser nanosurgery of cells and tissues. Appl Phys B-Lasers Optics 2005;81(8):1015–1047.
5. Schaffer CB, Brodeur A, Garcia JF, Mazur E. Micromachining bulk glass by use of femtosecond laser pulses with nanojoule energy. Opt Lett 2001;26(2):93–95.
6. Loesel FH, Fischer JP, Gotz MH, Horvath C, Juhasz T, Noack F, Suhm N, Bille JF. Non-thermal ablation of neural tissue with femtosecond laser pulses. Appl Phys B-Lasers Optics 1998;66(1):121–128.
7. Schaffer CB, Nishimura N, Glezer EN, Kim AMT, Mazur E. Dynamics of femtosecond laser-induced breakdown in water from femtoseconds to microseconds. Optic Express 2002; 10(3):196–203.
8. Konig K, Riemann I, Fritzsche W. Nanodissection of human chromosomes with near-infrared femtosecond laser pulses. Opt Lett 2001;26(11):819–821.
9. Chung SH, Clark DA, Gabel CV, Mazur E, Samuel ADT. The role of the AFD neuron in C-elegans thermotaxis analyzed using femtosecond laser ablation. Bmc Neurosci 2006;7: 30–41.
10. Yanik MF, Cinar H, Cinar HN, Chisholm AD, Jin YS, Ben-Yakar A. Neurosurgery—functional regeneration after laser axotomy. Nature 2004;432(7019):822–822.
11. Supatto W, Debarre D, Moulia B, Brouzes E, Martin JL, Farge E, Beaurepaire E. *In vivo* modulation of morphogenetic movements in Drosophila embryos with femtosecond laser pulses. Proc Natl Acad Sci U S A 2005;102(4):1047–1052.
12. Shen N, Datta D, Schaffer CB, LeDuc P, Ingber DE, Mazur E. Ablation of cytoskeletal filaments and mitochondria in live cells using a femtosecond laser nanoscissor. Mech Chem Biosyst 2005;2(1):17–25.
13. Kumar S, Maxwell IZ, Heisterkamp A, Polte TR, Lele TP, Salanga M, Mazur E, Ingber DE. Viscoelastic retraction of single living stress fibers and its impact on cell shape, cytoskeletal organization, and extracellular matrix mechanics. Biophys J 2006;90(10):3762–3773.
14. Tirlapur UK, Konig K. Targeted transfection by femtosecond laser. Nature 2002;418(6895):290–291.
15. Stevenson D, Agate B, Tsampoula X, Fischer P, Brown CTA, Sibbett W, Riches A, Gunn-Moore F, Dholakia K. Femtosecond optical transfection of cells: viability and efficiency. Opt Express 2006;14(16):7125–7133.
16. Juhasz T, Frieder H, Kurtz RM, Horvath C, Bille JF, Mourou G. Corneal refractive surgery with femtosecond lasers. IEEE J Sel Top Quant 1999;5(4):902–910.
17. Plamann K, Aptel F, Arnold CL, Courjaud A, Crotti C, Deloison F, Druon F, Georges P, Hanna M, Legeais JM, Morin F, Mottay E, Nuzzo V, Peyrot DA, Savoldelli M. Ultrashort pulse laser surgery of the cornea and the sclera. J Opt-Uk 2010;12(8):1–30.
18. Nishimura N, Schaffer CB, Friedman B, Tsai PS, Lyden PD, Kleinfeld D. Targeted insult to subsurface cortical blood vessels using ultrashort laser pulses: three models of stroke. Nat Methods 2006;3(2):99–108.
19. Sacconi L, O'Connor RP, Jasaitis A, Masi A, Buffelli M, Pavone FS. *In vivo* multiphoton nanosurgery on cortical neurons. J Biomed Opt 2007;12(5):050502.

20. Nishimura N, Schaffer CB, Friedman B, Lyden PD, Kleinfeld D. Penetrating arterioles are a bottleneck in the perfusion of neocortex. Proc Natl Acad Sci U S A 2007; 104(1):365–370.
21. Feng G, Mellor RH, Bernstein M, Keller-Peck C, Nguyen QT, Wallace M, Nerbonne JM, Lichtman JW, Sanes JR. Imaging neuronal subsets in transgenic mice expressing multiple spectral variants of GFP. Neuron 2000;28(1): 41–51.
22. Vogel A, Noack J, Nahen K, Theisen D, Busch S, Parlitz U, Hammer DX, Noojin GD, Rockwell BA, Birngruber R. Energy balance of optical breakdown in water at nanosecond to femtosecond time scales. Appl Phys B-Lasers Optics 1999;68(2):271–280.
23. Kleinfeld D, Mitra PP, Helmchen F, Denk W. Fluctuations and stimulus-induced changes in blood flow observed in individual capillaries in layers 2 through 4 of rat neocortex. Proc Natl Acad Sci U S A 1998;95(26):15741–15746.
24. Horecker BL. The absorption spectra of hemoglobin and its derivatives in the visible and near infra-red regions. J Biol Chem 1943;148(1):173–183.
25. Tsai PS, Friedman B, Ifarraguerri AI, Thompson BD, Lev-Ram V, Schaffer CB, Xiong Q, Tsien RY, Squier JA, Kleinfeld D. All-optical histology using ultrashort laser pulses. Neuron 2003;39(1):27–41.
26. Wray S, Cope M, Delpy DT, Wyatt JS, Reynolds EOR. Characterization of the near-infrared absorption-spectra of cytochrome-Aa3 and hemoglobin for the non-invasive monitoring of cerebral oxygenation. Biochim Biophys Acta 1988;933(1):184–192.
27. Smith RC, Baker KS. Optical-properties of the clearest natural-waters (200–800 Nm). Appl Optics 1981;20(2):177–184.
28. Theer P, Hasan MT, Denk W. Two-photon imaging to a depth of 1000 mu m in living brains by use of a Ti: Al2O3 regenerative amplifier. Opt Lett 2003;28(12):1022–1024.
29. Docchio F, Sacchi CA, Marshall J. Experimental investigation of optical breakdown thresholds in ocular media under single pulse irradiation with different pulse durations. Lasers Opthalmology 1986;1:83–93.
30. Kobat D, Durst ME, Nishimura N, Wong AW, Schaffer CB, Xu C. Deep tissue multiphoton microscopy using longer wavelength excitation. Opt Express 2009;17(16):13354–13364.
31. Rosen AD, Frumin NV. Focal epileptogenesis after intracortical hemoglobin injection. Exp Neurol 1979;66(2):277–284.
32. Lubatschowski H, Heisterkamp A, Will F, Singh AI, Serbin J, Ostendorf A, Kermani O, Heermann R, Welling R, Ertmer W. Medical applications for ultrafast laser pulses. RIKEN Review 2003;50:113–118.
33. Morrell F, Kanner AM, de Toledo-Morrell L, Hoeppner T, Whisler WW. Multiple subpial transection. Adv Neurol 1999;81:259–270.
34. Kaufmann WE, Krauss GL, Uematsu S, Lesser RP. Treatment of epilepsy with multiple subpial transections: an acute histologic analysis in human subjects. Epilepsia 1996;37(4): 342–352.
35. Wyler AR, Wilkus RJ, Rostad SW, Vossler DG. Multiple subpial transections for partial seizures in sensorimotor cortex. Neurosurgery 1995;37(6):1122–1127.
36. Stead M, Bower M, Brinkmann BH, Lee K, Marsh WR, Meyer FB, Litt B, Van Gompel J, Worrell GA. Microseizures and the spatiotemporal scales of human partial epilepsy. Brain 2010;133(9):2789–2797.
37. Krishnamurthy S, Powers SK. Lasers in neurosurgery. Laser Surg Med 1994;15(2):126–167.